# From Coherence to Function: Exploring the Connection in Chemical Systems

Shahnawaz R. Rather,\*,1 Gregory D. Scholes,\*,2 Lin X. Chen\*,3,4

<sup>1</sup>Department of Chemistry, University of Kentucky, Lexington, KY - 40506

<sup>2</sup>Department of Chemistry, Princeton University, Princeton, NJ - 08541

<sup>3</sup>Department of Chemistry, Northwestern University, Evanston, IL 60204

<sup>4</sup>Chemical Science and Engineering Division, Argonne National Laboratory, Lemont, IL 60439

Conspectus: The role of quantum mechanical coherences or coherent superposition states in excited state processes has received considerable attention in the last two decades largely due to advancements in ultrafast laser spectroscopy. These coherence effects hold promise for enhancing the efficiency and robustness of functionally relevant processes, even when confronted with strong energy disorder and environmental fluctuations. Understanding coherence deeply drives us to unravel mechanisms and dynamics controlled by order and synchronization at a quantum mechanical level, envisioning optical control of coherence to enhance functions or create new ones in molecular and material systems. In this frontier, the interplay between electronic and vibrational dynamics, specifically the influence of vibrations in directing electronic dynamics, has emerged as the leading principle. Here, two energetically disparate quantum degrees of freedom work in-sync to dictate the trajectory of an excited state reaction. Moreover, with the vibrational degree being directly related to the structural composition of molecular or material systems, new molecular designs could be inspired by tailoring certain structural elements.

In the realm of chemical kinetics, our understanding of the dynamics of chemical transformations is underpinned by fundamental theories such as transition state theory, activated rate theory, and Marcus theory. These theories elucidate reaction rates by considering the energy barriers that must be overcome for reactants to transform into products. Those barriers are surmounted by the stochastic nature of energy gap fluctuations within reacting systems, emphasizing that the reaction coordinate—the pathway from reactants to products—is not rigidly defined by a specific vibrational motion but encompasses a diverse array of molecular motions. While less is known about the involvement of specific intramolecular vibrational modes, their significance in certain cases cannot be overlooked.

In this Account, we summarize key experimental findings that offer deeper insights into the complex electronic-vibrational trajectories encompassing excited states afforded from state-of-the-art ultrafast laser spectroscopy in three exemplary processes: photo-induced electron transfer, singlet-triplet intersystem crossing, and intramolecular vibrational energy flow in molecular systems. We delve into rapid decoherence—loss of phase and amplitude correlations—of vibrational coherences along promoter vibrations during a sub-picosecond intersystem crossing dynamics in a series of binuclear platinum complexes. This rapid decoherence illustrates the vibration-driven reactive pathways from Franck-Condon state to the curve crossing region. We also explore the generation of new vibrational coherences induced by impulsive reaction dynamics—rather than by the laser pulse—in these systems, which sheds light on specific energy dissipation pathways and thereby on the progression of the reaction trajectory in the vicinity of the curve crossing on the product side. Another property of vibrational coherences, amplitude, reveals how energy can flow from one vibration to another in the electronic excited state of a terpyridine-molybdenum complex hosting a nonreactive dinitrogen substrate. A slight change in vibrational energy triggers a quasi-resonant interaction, leading to constructive wavepacket interference and ultimately intramolecular vibrational redistribution from a Franck-Condon active terpyridine vibration to dinitrogen stretching vibration, energizing the dinitrogen bond.

# **KEY REFERENCES**

• Rather, S. R.; Weingartz, N. P.; Kromer, S.; Castellano, F. N.; Chen, L. X. Spin-vibronic coherence drives singlet-triplet conversion. *Nature* **2023**, *620* (7975), 776-781. This work describes intersystem crossing

- dynamics in a series of synthetic binuclear platinum complexes as driven by a coupled spin-orbit and vibronic effects utilizing inter-platinum vibration as an energy tuning degree of freedom.
- Rather, S. R.; Fu, B.; Kudisch, B.; Scholes, G. D. Interplay of vibrational wavepackets during an ultrafast electron transfer reaction. *Nat. Chem.* **2021**, *13* (1), 70-76.<sup>2</sup> This work describes a complex electron transfer reaction trajectory in the Marcus-inverted region composed of multiple vibrational coordinates that progressively drive the reactants to the transition state region and prevent the recurrence of the reactant state.
- Rather, S. R.; Bezdek, M. J.; Chirik, P. J.; Scholes, G. D. Dinitrogen Coupling to a Terpyridine-Molybdenum Chromophore Is Switched on by Fermi Resonance. *Chem* **2019**, *5* (2), 402-416.<sup>3</sup> This work describes a case of accidental quasi-resonance between quantum vibrations as an outcome of isotopic substitution in a metal complex and how that introduces vibrational coupling and wavefunction delocalization prompting selective vibrational energy flow for bond activation.

### 1. INTRODUCTION

Many chemical reactions, including electron transfer, happen because of barrier crossings enabled by a huge number of degrees of freedom that collectively produce a single "reaction coordinate". However, in many instances of photoinduced dynamics intramolecular vibrational modes provide additional, specific, reaction coordinates. Examples include radiationless transitions and electron transfer in the Marcus "inverted regime". These intramolecular reaction coordinates are interesting because they can be controlled by molecular design—thus offering a way to influence ultrafast dynamics by chemical design.

Light-induced excited state processes in systems ranging from small molecules to materials and proteins are ubiquitous, and relevant to applications like solar energy capture and conversion, optoelectronics, photosensitization, molecular photonics and electronics, photocatalysis, quantum information etc. 11-17 In the last two decades, with the advent of multi-dimensional ultrafast time-resolved techniques capable of performing measurements on ultrafast time scales and broader energy scales, the observation of persistent oscillatory third-order signals in biological, molecular, and material systems indicated the necessity to invoke the relevance of functional quantum effects. <sup>1-3, 18-24</sup> In particular, synchronization and coherence conceptually, oscillations in lock step—on the microscopic scale has been suggested to influence the effectiveness of many important processes. For example, Cerullo and coworkers elucidated the role of vibrations in ultrafast conical intersection dynamics of retinal chromophore, a step in the visual transduction cascade.<sup>25</sup> This was further complemented by Miller and coworkers, who recovered a host of local vibrational modes that actively drive the formation of conical intersection in Rhodopsin. <sup>26</sup> Similarly, conical intersection dynamics was shown to synchronize the ultrafast singlet fission process in pentacene dimers.<sup>27</sup> Vibronic coupling is considered integral to energy transfer and charge separation in photosynthetic systems. <sup>28, 29</sup> Electron-vibrational coupling was shown to induce a delocalization of electronic wavefunction across the interface of a heterojunction, and the correlated electronic-vibrational motion results in early time ultrafast charge separation. 18, 30 In general, the coupling of vibrational and electronic degrees drives charge and exciton generation, carrier separation, transport and recombination in photovoltaic materials.<sup>2</sup> 19, 27, 31, 32

Central to many studies of ultrafast coherence phenomena, are intramolecular vibrations of molecules. In recent work, we have been interested in trying to follow various of these intramolecular reaction coordinates using femtosecond broadband spectroscopies. Our goal is to identify the vibrations that promotes ultrafast dynamics, examine the interplay of various vibrations, and to look for evidence of significant effects beyond the Born-Oppenheimer approximation that influence dynamics on approach to a transition state. This latter goal remains an open challenge. Our approach, described below, is to use vibronic wavepackets as a probe, from the molecular perspective, of the way reaction coordinates evolve during the course of photoinduced dynamics. Here, we will illustrate the idea and our progress with three specific examples.

Briefly, ultrafast laser spectroscopy experiments employing sub-10 femtosecond laser pulses bring us to a unique spectral and temporal jurisdiction where a pump pulse can populate excited states electronically

while simultaneously creating coherent superpositions of vibrational states along numerous displaced vibrational degrees of freedom.<sup>33-35</sup> The latter are identified as vibrational coherences or wavepackets, which imprint their signature on the non-linear third-order electronic signal by modulating its amplitude periodically. The time-dependent behavior of vibrational coherences can be described predominantly classically like a pendulum, however, what we imagine is that changes in the wavepacket properties might indicate vibronic coupling effects as the reactant and product potentials become near-resonant at the curve crossing. Putting it into perspective, the reactant and acceptor potentials may be local at their equilibrium positions, but the curve crossing region can be adiabatic, and hence the reactive trajectory may repeatedly pass from a localized basis to delocalized basis as a function of vibronically coupled nuclear coordinate. Figure 1 illustrates the experimental strategy implemented, where we measure and characterize wavepacket dynamics on the reactant and product states by monitoring reactant and product transient absorption signals. A major aspect of that characterization typically hinges on distinguishing promoter coherences from spectator coherences and tracking their wavepacket properties, such as dephasing, amplitude, and lineshapes as the reactants transform intro products. As an example, in a conical intersection, the energy tuning and coupling vibrations can be classified as promoter vibrations.

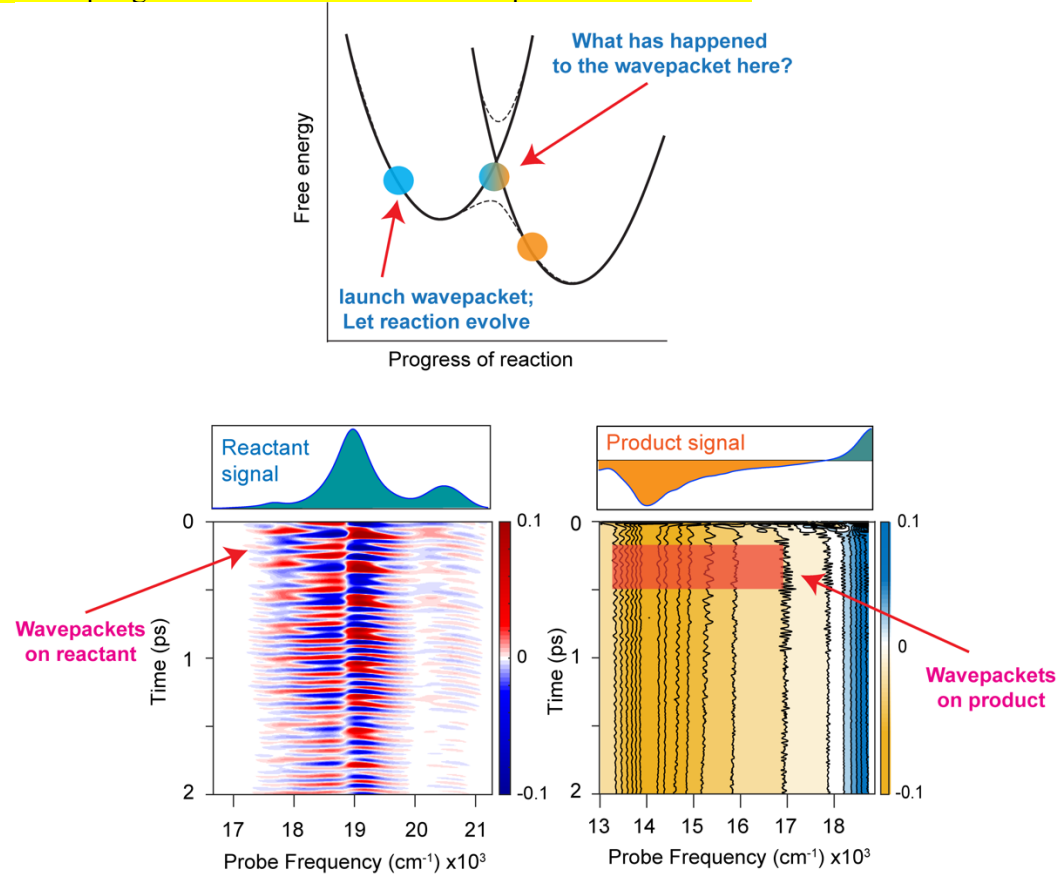


Figure 1. A schematic representation of the experimental strategy implemented to deduce the role of vibrational motion as potent reaction coordinates. The strategy involves launching wavepackets on the reactant state and subsequently tracking wavepacket motion on the reactant and product states, and predict how vibrations drive the crossing between reactant and product surfaces by exploiting the dynamical changes that wavepacket undergoes. The transient absorption maps are plotted as  $\Delta T/T$ . The bottom two panels are partially adapted from ref. 2, Nature Publishing Group.

In this Account, we review some of the recent discoveries that uncover how vibrational coherences sense complex reactive trajectories in excited states and inform on the role of vibronic effects in functionally relevant transformations. We will discuss how decoherence is a characteristic signature of vibrational

coupling to electronic dynamics, informing on the reaction trajectory in a singlet-triplet conversion dynamics occurring on femtosecond timescale. We will describe another signature of coherences—manifested through coherence regeneration—informing on the energy dissipation mechanism via vibrational excitation of modes coupled to the electronic dynamics. The sensitivity of vibrational coherences to slight change in energy levels—particularly in the case of energy levels approaching quasi-resonance—will also be discussed through the lens of redistribution of probability amplitude and interference of wavepackets over spatially disparate molecular entities.

# 2. REACTION-DRIVEN DECOHERENCE OF VIBRATIONAL COHERENCES

In a conventional broadband pump-probe (BBPP) based spectroscopy, where superpositions of vibrational states are created by impulsive excitation using short resonant pump pulses, decoherence refers to the loss of such vibrational or vibronic superpositions. Typically, vibrational superpositions in the Born-Oppenheimer limit exhibit a picosecond long decoherence. <sup>33, 36-38</sup> However, in the non-Born-Oppenheimer limit, due to nonadiabatic electron-nuclear coupling, superposition states along the vibronic coupling coordinate can undergo enhanced decoherence. For example, the rapid loss of vibrational phase coherence has been a signature of vibrationally-driven *trans-cis* isomerization in rhodopsin—the primary step in the photochemistry of vision. The three reaction promoting vibrations—ethylenic stretch vibration, hydrogenout-of-plane wagging mode, and a localized torsion at 11-position double bond dephase on the order of both the excited state lifetime and the observed photoproduct formation. <sup>39</sup> This is one of the crucial representation of how vibrational decoherence informs on the vibronic nature of structural transformation in rhodopsin. The dynamics is typical of multimodal conical intersection that funnel excited state population to lower states at an extremely rapid rate. <sup>40</sup>

A phenomenon similar to the vibronic mechanism but operating on electronic states of different spin-multiplicities, has been theorized since the 1960's to be responsible for rapid intersystem crossing (ISC) in molecular systems. This phenomenon is called the spin-vibronic mechanism (SVM).<sup>41, 42</sup> In simpler words, while a conventional vibronic mechanism leads to singlet-singlet or triplet-triplet radiationless transitions, SVM, on the contrary, leads to singlet-triplet or triplet-singlet radiationless transitions. The SVM mechanism draws its significance from its ability to synchronize relativistic and non-relativistic quantum effects, enabling rapid ISC. Typically, we understand ISC to be an outcome of spin-orbit coupling induced by heavy atom effect, which renders an otherwise quantum mechanically forbidden transition allowed through higher-order mixing of electronic states. In certain instances, however, vibrational degrees of freedom couple with electronic dynamics and work in-sync with spin-orbit effect, thereby introducing further mixing of electronic states of different spin-multiplicity to enable spin-vibronic-mediated ISC.<sup>1, 42</sup>

As indicated above, a theoretical foundation of SVM has existed for many decades, but aside from some experimental studies that indirectly support SVM, concrete experimental evidence proving SVM was lacking. 42-47 In Rather et al, SVM was demonstrated by tracking decoherence of a vibrational wavepacket during ISC in a series of four structurally related binuclear Pt(II) metal-metal-to-ligand charge-transfer (MMLCT) complexes using pump-probe and two-dimensional electronic spectroscopies. At sufficiently short inter-Pt(II) distances in these dimeric complexes, the  $\sigma$ -interactions between the  $5d_z^2$  orbitals of Pt(II) lead to MMLCT transitions, whose resonant photoexcitation launches a vibrational wavepacket along the Pt–Pt internuclear axis in the singlet manifold. 48 Of the four complexes, Pt1 (Fig. 2a) exhibited two distinct vibrational coherences, in the region of Pt–Pt stretching frequency, that peak at 107 and 147 cm<sup>-1</sup> frequencies (Fig. 2b-d). The Pt2 complex exhibited a peak at 112 cm<sup>-1</sup> frequency, but instead of a distinct peak at around ~150 cm<sup>-1</sup> like that in Pt1, a broad attenuated feature to the higher-frequency side of 112 cm<sup>-1</sup> peak was observed. The ground or excited state origin of these vibrational coherences were identified primarily by monitoring the intensity of Fourier transform bands under positively and negatively chirped laser-pulse excitation. The band at around 110 cm<sup>-1</sup> originates from the ground electronic state, and the band (shoulder in the case of Pt2) around 150 cm<sup>-1</sup> originates from the excited singlet electronic state, which was

further supported by reconstructing two-dimensional spectral beat maps and mapping the distribution of peak amplitude along the probe frequency in BBPP spectroscopy (Fig. 2d).<sup>1</sup> The higher vibrational frequency observed in the excited electronic state is due to shortening of the Pt–Pt bond by approximately 0.25Å during the photoexcitation of the singlet MMLCT transition.<sup>48</sup>

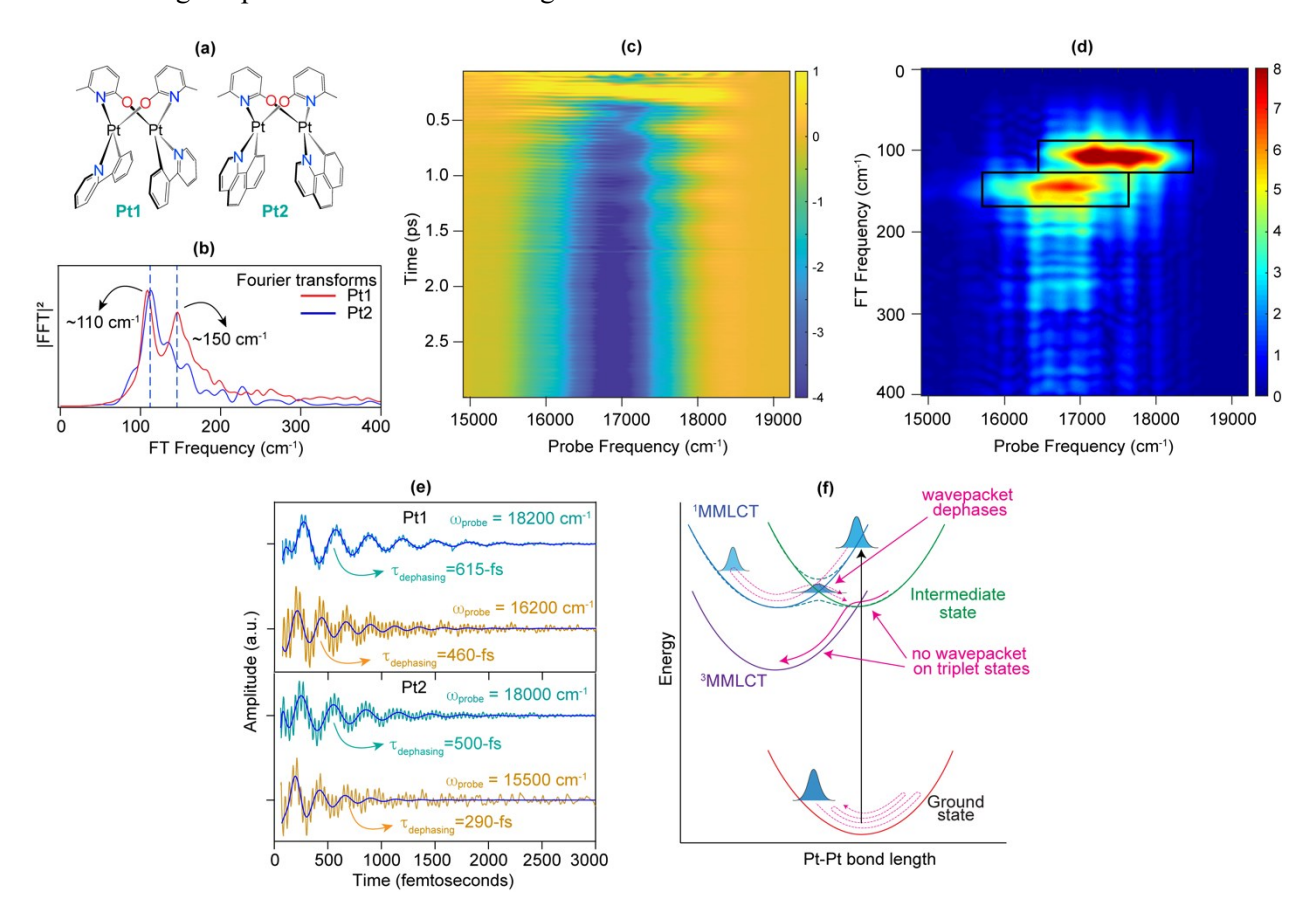


**Figure 2.** (a) Molecular structures of **Pt1** and **Pt2**. (b) Fourier transform spectra of time-domain wavepacket oscillations of **Pt1** and **Pt2** integrated over all probe frequencies and normalized at the peak intensity. (c) A representative BBPP map of **Pt1** (ΔT/T) showing wavepacket oscillations superimposed on its electronic transient absorption signals along the time axis. The color scale represents the difference in the intensity of the probe pulse spectrum in the presence and absence of a pump pulse. The transient signal in this spectral region is dominated by triplet excited state absorption. (d) A Fourier transform map of the corresponding time-domain oscillations in the oscillatory frequency region of 0-400 cm<sup>-1</sup>. (e) Time-domain oscillatory signals of **Pt1** and **Pt2** at the indicated probe frequencies fitted by exponentially decaying cosine functions. The rapidly oscillating component is due to the tetrahydrofuran solvent Raman mode of frequency, around 913 cm<sup>-1</sup>. (f). Conical intersection depicted between the singlet and triple intermediate state as a function of Pt–Pt vibrational coordinate. The Pt–Pt wavepacket generated on the <sup>1</sup>MMLCT state due to photoexcitation dephases during the ISC process between the singlet to triplet states. A corresponding wavepacket generated on the ground state which oscillates with ~110 cm<sup>-1</sup> is also shown. No wavepacket was observed on the triplet states. Panel (a, b, d, e, f) are adapted from ref. 1, Nature Publishing Group.

The role of the Pt–Pt vibrational motion in the SVM was predominantly deciphered from the decoherence of its wavepacket in-sync with ISC between singlet and triplet MMLCT manifolds in these complexes. A nonlinear least-squares fitting—using exponentially decaying cosine functions—of the experimentally obtained time-domain wavepacket oscillations (Fig. 2e) revealed dephasing time-constants of 615±60 fs and 460±40 fs respectively, for the ground and singlet excited state vibrational coherences at 107 and 147 cm<sup>-1</sup> for Pt1. For Pt2, the respective ground and excited state dephasing time constants of 505±55 fs and 290±40 fs were obtained. The dephasing times of these vibrational coherences from Lorentzian lineshape

fitting were within about 60 fs of the above time constants. Our results explicitly indicated that the Pt–Pt vibrational coherence of the <sup>1</sup>MMLCT state dephases faster than the corresponding ground state coherence (Fig. 2e). In fact, the rate of vibrational dephasing follows the same trend as the ISC rate from the singlet to triplet manifold, reported previously. <sup>49</sup> Despite the ISC rate being fast, the singlet excited state vibrational coherence does not transfer to the triplet state, unlike previously observed in other similar complexes, for instance, [Pt<sub>2</sub>(pop)<sub>4</sub>]<sup>4-</sup> (where pop is pyrophosphate). <sup>50</sup> In other words, the Pt–Pt vibrational coherence became wholly attenuated in the <sup>1</sup>MMLCT states, at the same rate as the ISC. This behavior is true for Pt3 and Pt4 as well (*vide infra*), where the <sup>1</sup>MMLCT vibrational coherences was no longer observed, instead a triplet wavepacket regenerated in the impulsive limit of ISC rate. <sup>1</sup>

The enhanced decoherence of the Pt-Pt vibrational mode in the excited state of the structural analogs of binuclear platinum complexes provides compelling evidence for the vibronically driven reaction trajectory from where the wavepacket was launched on the singlet state to where this state crosses with the triplet state. If the two states were to cross as pure diabats, then at the crossing point the singlet state instantly transitions to a triplet state with a significantly short singlet-triplet coherence time, the vibrational wavepacket generated on the singlet state will continue to maintain its coherence on the triplet state as a spectator mode. Considering that the lowest triplet state has a contracted Pt–Pt bond distance, the wavepacket on the triplet state must dephase with a longer decoherence time, longer than the ground state. This would be akin to Born-Oppenheimer separation of electronic and vibrational wavefunctions during the ISC transition. However, we do not observe Pt-Pt wavepacket on the triplet state. What that potentially points out is the presence of a significant adiabaticity in the vicinity of the curve crossing between the singlet and triplet states (Fig. 2f). Therefore, the transition of an electron from singlet to triplet state is not instantaneous, instead, due to adiabaticity, the decoherence of the singlet-triplet mixed state is relatively slowed down by vibronic coupling. Thus, the system trajectory from where the wavepacket is generated smoothly transitions from a singlet only state to a vibronically-mediated mixture of singlet and triplet states. This evolution results in change in the symmetry character of the vibronic states as a function of vibronic coordinate, and additionally increases anharmonicity near the seam of the conical intersection, leading to loss in the phase coherence of vibrational states along the vibronically coupled coordinate. 51 Additionally, considering that all the complexes have same number of centrally positioned platinum atoms, the spin-orbit effect would be similar in all of them, but still observing different ISC and wavepacket dynamics indicates a significant role of vibronic coupling mediate ISC.

### 3. EMERGENCE OF VIBRATIONAL COHERENCES DRIVEN BY REACTIVE DYNAMICS

A relatively uncommon phenomenon pertaining to certain reactions is the emergence of a coherent superposition state, not by the direct laser excitation as encountered usually in coherent spectroscopies, but an outcome of reactive dynamics. This rare occurrence brings forth certain elements of multidimensional reactive trajectories which would otherwise remain obscure. The beauty of such phenomenon is that it allows us to zoom into the region to the product side of curve crossing and relays back how the activated state or transition state dissipates energy to favor product formation.

In Electron Transfer Reactions. Our earlier attempts to use vibrational superposition states as a reporter of the electron transfer dynamics were met with challenges, mostly due to either desired spectral signatures being out of the experimental probe spectral window or the rate of ET reaction being slower or comparable to the vibrational dephasing times.<sup>37, 52</sup> These challenges were overcome by identifying the right choice of electron acceptor and electron donor system, namely N,N'-bis(2,6-methylphenyl)perylene-3,4,9,10-tetracarboxylic diimide (PDI) in N,N-dimethylaniline (DMA), which yielded a superfast rate of ET reaction and transient signatures that could be probed in the visible spectral window (Fig. 3a).<sup>2</sup> The ET reaction between electron acceptor, PDI, dissolved in an electron donor solvent, DMA, is prompted by the photoexcitation of PDI, and occurs in approximately 30 fs. The large driving force in comparison to the reorganization energy places this reaction deep within the Marcus inverted region, and the superfast rate of

ET reaction indicates that solvent degree of freedom is effectively frozen. To justify the extraordinarily fast reaction rate than predicted by the Marcus theory, Jortner and Bixon<sup>53</sup> early on theorized the role of high-frequency promoter vibrations that provide "nesting" of free energy curves. The multiple crossings in the nest occur between the reactant and product free energy curves at energy positions equivalent to the vibrational ladder of the respective quantum modes.<sup>2, 10</sup> This phenomenon furnishes multiple reaction crossing pathways in the barrierless and near-barrierless regime between reactant and product states. The overall ET rate is expressed as a summation over electron transfer rates along each individual reactant product free energy curve crossing. A significant attenuation of high-frequency vibrational coherences, specifically for the 1308 and 1599 cm<sup>-1</sup> modes, was monitored in the excited state transient absorption signal of PDI when photoexcited in the presence of the electron donating solvent, DMA (Fig. 3b).<sup>2</sup> A similar decoherence behavior emerged in another electron transfer system where the electron acceptor was substituted with bis(phenylethynyl)-naphthacene alongside various electron donating solvents.<sup>54</sup> In this system, dephasing dynamics of 11 vibrational wavepackets were analyzed, revealing that multiple vibrational modes decohered simultaneously in tune with electron transfer rates.

In the example of PDI in DMA, new wavepacket oscillations in the product transient signal (PDI radical anion more precisely) with a peak frequency of ~313 cm<sup>-1</sup> (along with a minor peak at ~90 cm<sup>-1</sup>) indicated the emergence of new vibrational coherences on the product state (Fig. 3c).<sup>2</sup> This new vibrational coherence is in contrast to the vast majority of spectator wavepackets (orthogonal to the reaction coordinate) observed on the product state that were generated by direct laser excitation in the reactant state. All control measurements confirmed that this newly generated wavepacket explicitly emerges only on the product state during the electron transfer reaction.<sup>2</sup> The seemingly counterintuitive emergence of a new wavepacket was hypothesized to be a outcome of how the PDI molecular structure suddenly reacts to the impulsive transfer of electron from the DMA donor. Our hypothesis envisioned a low-frequency vibrational mode of frequency 313 cm<sup>-1</sup> that undergoes abrupt shift in its equilibrium coordinate position at the onset of the electron transfer event (Fig. 3d). This abrupt shift in its equilibrium position leads to quantum beats as a consequence of the coherent superposition state along this mode on the product state. In a musical analogy, imagine plucking a guitar string and then abruptly changing the tuning peg to a different pitch. The string will oscillate with a large amplitude at the new pitch. Here the oscillation of the string represents the vibration and the change in the tuning peg represents the electron transfer event.

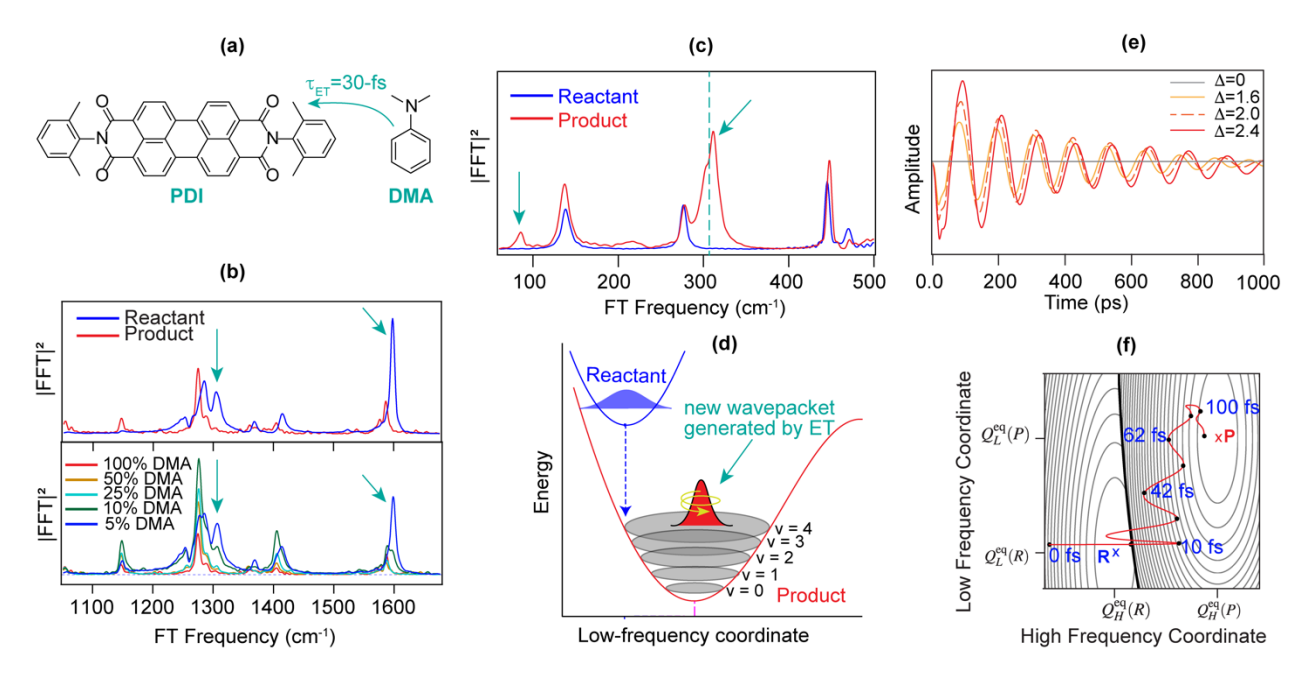


**Figure 3.** (a) Molecular structures of electron acceptor, PDI, and electron donor, DMA. (e) Integrated Fourier transform spectra of the excited state absorption signal of PDI in THF solvent, shown in the blue trace, and the product state signal of PDI in the electron donating solvent, shown in the red trace, in the high frequency 1,000-1,700 cm<sup>-1</sup> region, depicting a diminishing signal along the indicated high-frequency modes. The bottom panel shows the Fourier transform spectra in a range of conditions differing in the ratio of DMA to THF which affects the rate of electron transfer reaction. (c) Integrated Fourier transform spectra of PDI in THF, shown in the blue trace, and PDI in DMA, shown in the red trace, transient absorption signals in the low frequency region, depicting the emergence of a new vibrational coherence in the product state. (d) An illustration of the mechanism that leads to coherent wavepacket generation along the low-frequency coordinate by impulsive electron transfer reaction. (e) Theoretical simulations depicting wavepacket generated oscillations on the product state for a non-zero displacement along low-frequency mode between reactant and product states. The amplitude of oscillations increases with an increase in the displacement. No oscillations were predicted with zero displacement between the reactant and product states along the low-frequency coordinate. (e) A two-dimensional contour map of reactant and product potentials along the high-and low-frequency coordinates, showing the averaged wavepacket position as a function of time as predicted by the Redfield theory. Panels (a-e) are adapted from ref. 2, Nature Publishing Group.

A multilevel Redfield theory<sup>55</sup> was implemented to provide theoretical insights into the emergence of the 313 cm<sup>-1</sup> vibrational wavepacket on the product state. The model comprised three electronic states (ground state, reactant state, and product state), with each state coupled to a generalized high-frequency mode and a low-frequency mode.<sup>2</sup> Taking inspiration from the experimental results, the reactant state was prepared such that it is displaced with respect to the ground state only along the high-frequency coordinate, and undisplaced along the low-frequency coordinate. The simulations indicated that when the product state has a zero displacement with respect to the reactant state along the low-frequency mode, no low-frequency wavepacket was generated on the product state (Fig. 3e). However, when the product state was prepared in a way such that it is displaced along the low-frequency coordinate from the reactant state, a new nonstationary wavepacket was generated on the product state indicated by the time-domain oscillatory signal (Fig. 3e). The amplitude of this wavepacket oscillations can be seen to increase when the product state has larger displacement. Furthermore, the phase of this nonstationary wavepacket on the product state was also predicted to have its initial phase shifted than the phase of the spectator-mode wavepackets, which was also confirmed by inverse-Fourier analysis of the experimentally obtained data.<sup>2</sup> Intuitively, as the ET reaction is driven by superfast motion along the high-frequency coordinate (with a time-period of ~20-fs), the product state in the curve crossing configuration space finds itself at a non-equilibrium, high energy position along the low-frequency mode, that results in coherent generation of the 313 cm<sup>-1</sup> vibrational wavepacket on the product state (Fig. 3f). The quasi-ballistic electron transfer event therefore acts like a short pulse impulsively generating a coherent wavepacket. The utility of probing the generation of this wavepacket is that it informs on the way energy is dissipated by the transition state in an irreversible manner such that coherent recurrence of the electron transfer is prohibited. Remarkably, this behavior can still be explained well within the limits of the Born-Oppenheimer framework, and the orthogonality of the high and low frequency vibrations.

In Singlet-Triplet ISC. A case of emergence of a vibrational coherence outside the framework of the Born-Oppenheimer approximation is demonstrated in light of the SVM in the binuclear platinum complexes, noted above. The signature of the emergence of vibrational coherence was found in two of the four complexes, Pt3 and Pt4 (Fig. 4a,b), which exhibited a narrow and intense Fourier transform band peaking at 145 and 148 cm<sup>-1</sup>, respectively (Fig. 4c). Interestingly, these frequency bands do not conform to the Lorentzian lineshape as is the case with typical Franck-Condon active wavepackets, instead, they are Gaussian in nature. Further, inverse Fourier analysis of these frequency bands indicated that instead of a monotonic decay, their oscillations exhibited an initial growth of approximately 800 fs followed by an exponential decay with a time constant of approximately 1 picosecond (Fig. 4d). This contrasts with the similar frequency wavepacket in Pt1 and Pt2, which exhibited a monotonic decay in the oscillation amplitude (Fig. 1e). These factors, besides many others, indicated that the generation and dissipation

mechanisms of these wavepackets in Pt3 and Pt4 were different from those in Pt1 and Pt2, despite all the complexes exhibiting similar overall excited state dynamics.

The emergence of the 145 and 148 cm<sup>-1</sup> vibrational coherences in Pt3 and Pt4 was found to occur due to nonadiabatic coupling between the <sup>1</sup>MMLCT state and the triplet manifold leading to conical intersectionmediated ISC (Fig. 4e). In effect, the rapid ISC process occurring on a timescale faster than 100-fs in Pt3 and Pt4 leads to rapid decoherence of the singlet Pt-Pt vibrational wavepacket of frequency around 150 cm<sup>-1</sup> due to strong nonadiabatic mixing of the singlet and triplet electronic states close to the Franck-Condon region. However, the ligand-centered triplet state—identified as a transitory intermediate triplet state having symmetry different from that of the singlet state and Pt-Pt equilibrium bond length longer than that in the singlet state, acts as the state where re-emergence of the decohered wavepacket occurs. This reemerged wavepacket on the intermediate state has a frequency of ~120 cm<sup>-1</sup> and goes away in ~300-fs in Pt3 and Pt4 in sync with the population leaking out of this state into the final <sup>3</sup>MMLCT state. The reemergence of the Pt-Pt wavepacket is due to the impulsive rate of the ISC with respect to period of the Pt-Pt vibration. The <sup>3</sup>MMLCT and <sup>1</sup>MMLCT states share the same symmetry, similar Pt–Pt equilibrium bond length, and same orbital; thus, the two states have negligible spin-orbit coupling with each other. Therefore, the <sup>3</sup>MMLCT state instead of receiving population directly from <sup>1</sup>MMLCT state, is populated indirectly from the vibronically coupled intermediate ligand-centered state via internal conversion. The Pt-Pt wavepacket that was impulsively generated in the intermediate triplet state transfers to the <sup>3</sup>MMLCT state as a consequence of electronic population transfer as evidenced by the growth of its time-domain oscillations over a timescale of 500-1000 fs (Fig 4d). This wavepacket upshifts its frequency from ~120 cm<sup>-1</sup> in the intermediate state to 145 cm<sup>-1</sup> (in Pt3) and 148 cm<sup>-1</sup> (in Pt4) in the <sup>3</sup>MMLCT state due to shortening of the bond length. Due to the contraction of the Pt-Pt bond length in the <sup>3</sup>MMLCT state, its vibrational coherence is projected high up the vibrational ladder which subsequently relaxes to the bottom of the well and dephases over a much longer timescale of 3-5 ps. The observed wavepacket dynamics fully corroborates with the theoretical potential energy state calculations of these complexes.<sup>49</sup>

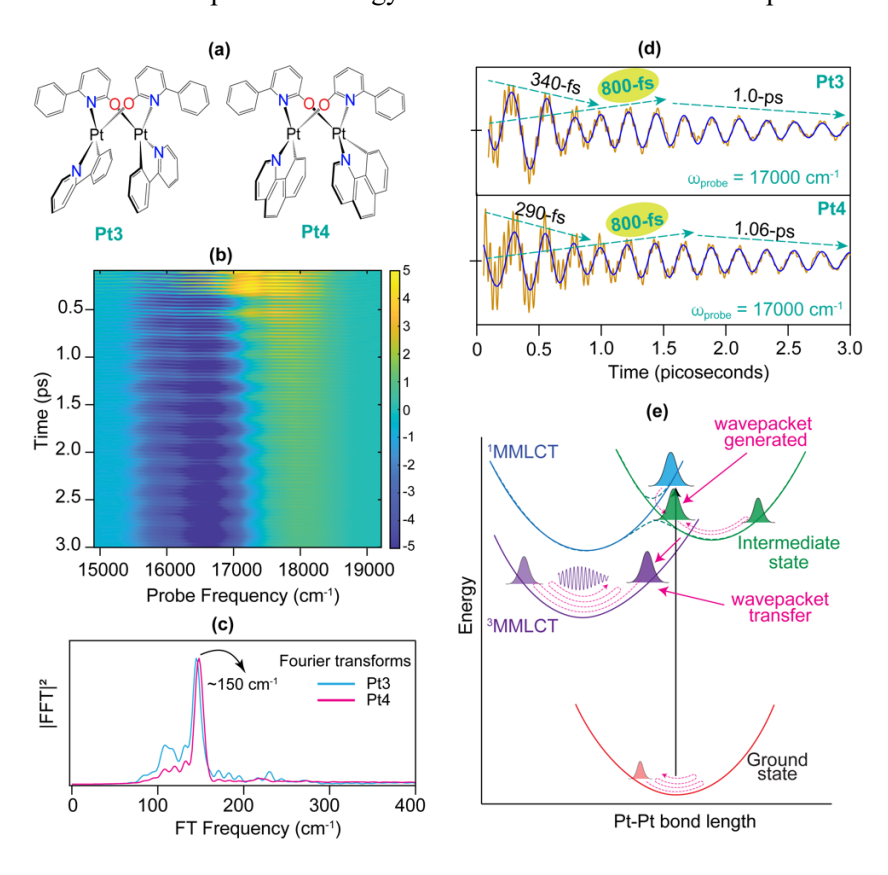


Figure 4. (a) Molecular structures of Pt3 and Pt4. (b) A representative BBPP map of Pt4 (ΔT/T) in THF solvent showing long-lived oscillations on the triplet absorption signal. (c) Fourier transform spectra integrated over all probe frequency of Pt3 and Pt4 transient spectra, depicting the narrow and intense band at ~150 cm<sup>-1</sup> frequency. The Fourier transform spectra are normalized to the peak intensity. (d) Nonlinear least squares fitting of the raw time-domain oscillations using three exponentially decaying cosine functions at a representative probe frequency (17000 cm<sup>-1</sup>) of Pt3 and Pt4. The dashed arrows overlayed on the two plots are guides to depict the decay (pointing downward) or growth (pointing upward) of the wavepacket amplitude. (e) Pt–Pt vibrational wavepacket dynamics during the spin-vibronic mechanism for Pt3 and Pt4. The curves are plotted to depict non-Born-Oppenheimer crossing of the singlet and intermediate triplet states medicated by the Pt–Pt vibrational coordinate via spin-vibronic coupling. All plots are adapted from ref. 1. Nature Publishing Group.

The unique shuttling of the wavepacket dynamics along the Pt–Pt stretching vibration directly alludes to the ISC being driven by vibrational motion leading up to the conical intersection. The re-emergence of wavepacket deciphers the rate at which the ISC process occurs with reference to the position of the curve crossing along the Pt–Pt stretching trajectory. In **Pt3** and **Pt4**, the generation of coherence due to nonadiabatic mixing of states indicates that mixing must occur closer to the Franck-Condon geometry. While in **Pt1** and **Pt2**, the absence of the generation of coherence indicates that the nonadiabatic mixing requires that the singlet state must evolve away from Franck-Condon geometry along the Pt–Pt coordinate. The position of the conical intersection—close to or away from the Franck-Condon region—could be related to the steric constraints introduced by the bridging ligands in these binuclear complexes. The bulkier bridging ligands introduce more constraint in the **Pt3** and **Pt4** complexes, favoring conical intersection close to the Franck-Condon region. This intricate electronic-vibrational interplay would not have come forth without the re-emergence of the Pt–Pt vibrational coherence.

The mechanisms leading to the generation/re-emergence of vibrational coherences in the two cases highlighted above may be somewhat different from each other: nesting of free energy curves in the case of electron transfer and spin-vibronic mixing of singlet and triplet states, but the implications and outcomes are vastly similar. Namely, there is an inevitable flow of energy at the transition state region from vibronic degree of freedom to reaction coordinate-coupled vibrations, creating instantaneous vibrational excitations that help dissipate energy and localize electron in the product state. This is typically the case with many reactions, but the generation of vibrational coherences within the impulsive timescale of the reaction is rare, and more so it informs us of the composition of reaction coordinate in the vicinity of the transition state.

# 4. COHERENCE AMPLITUDE REDISTRIBUTION DRIVEN BY QUASI-RESONANT INTERACTION

Vibrational coherences, besides sensing instantaneous changes in the coupled electronic-vibrational dynamics and relaying that via their decoherence or reemergence of coherence, also sense slight changes in the vibrational energy elsewhere.<sup>3</sup> This has implications for directed energy flow and selective bond activation. Our work described how Fermi-resonance coupling of vibrations links spatially disparate light-absorbing parts of a metal complex to potential reaction site.<sup>3</sup> This mechanism couples vibrational motions of a metal complex for directed energy flow and prevents incoherent loss of energy. The effect became apparent when vibrational coherence underwent amplitude redistribution in a metal complex during isotopic substitution at the dinitrogen reaction site. The complex investigated was an end-on dinitrogen-bridged bimetallic molybdenum complex, having a light-absorbing molybdenum terpyridine chromophore and a bridging dinitrogen ligand as a potential reaction site (Fig 5a). The photophysical Jablonski model of the complex was described previously.<sup>56</sup>

The isotopic substitution at the dinitrogen site from the lighter dinitrogen,  $^{14}N_2$ , to heavier dinitrogen,  $^{15}N_2$ , leads to a shift of the wavepacket frequency from 1565 cm<sup>-1</sup> to 1515 cm<sup>-1</sup> (Fig. 5b). None of the remaining low- or high-frequency vibrational coherences showed any observable shift, clearly indicating that this normal mode is a highly localized N=N stretching vibration. The downshift of the stretching frequency owing to substitution by the heavier nitrogen atoms simultaneously led to a significant enhancement in the

intensity of another peak with frequency positioned between  $^{14}N_2$  and  $^{15}N_2$  dinitrogen frequencies (Fig. 5b). The intensity of this frequency band at 1535 cm<sup>-1</sup> in the  $^{15}N_2$  complex was approximately 4-times higher than that in the  $^{14}N_2$  complex. This enhancement in the 1535 cm<sup>-1</sup> peak occurred concurrently with a slight decrease in the intensity of the 1515 cm<sup>-1</sup> peak.

The electronic structure calculations of this complex revealed that the 1535 cm<sup>-1</sup> mode is a delocalized inplane breathing vibration of the terpyridine ligands.<sup>3</sup> It is noteworthy that during photoexcitation, the electron is removed from a molecular orbital that is not a purely metal-centric orbital; instead, it is delocalized over the two metal centers and dinitrogen moiety.<sup>56, 57</sup> The highest occupied molecular orbital exhibits both N=N bonding and Mo-N anti-bonding character. Thus, transition of the electron from the Mo-N=N-Mo-based orbital to the terpyridine  $\pi^*$  orbital renders both the dinitrogen stretching vibration and the terpyridine in-plane breathing vibration Franck-Condon active, generating displaced wavepackets along these modes in the photoexcited state.<sup>3</sup> The insensitivity of the vibrational frequency of the in-plane terpyridine mode to the isotopic substitution at the dinitrogen site suggested that the two vibrational modes are not coupled through reduced mass via sharing common atoms. The theoretical calculations further predicted that dinitrogen isotopic substitution leads to enhancement of the displacement vectors associated with the in-plane breathing vibration of the terpyridine ligands (Fig. 5c).<sup>3</sup> This led us to hypothesize that instead of sharing mass, the two high-frequency quantum vibrations are energetically coupled with each other, and that is the origin of the amplitude enhancement effect we observed in the pump-probe experiments.<sup>3</sup>

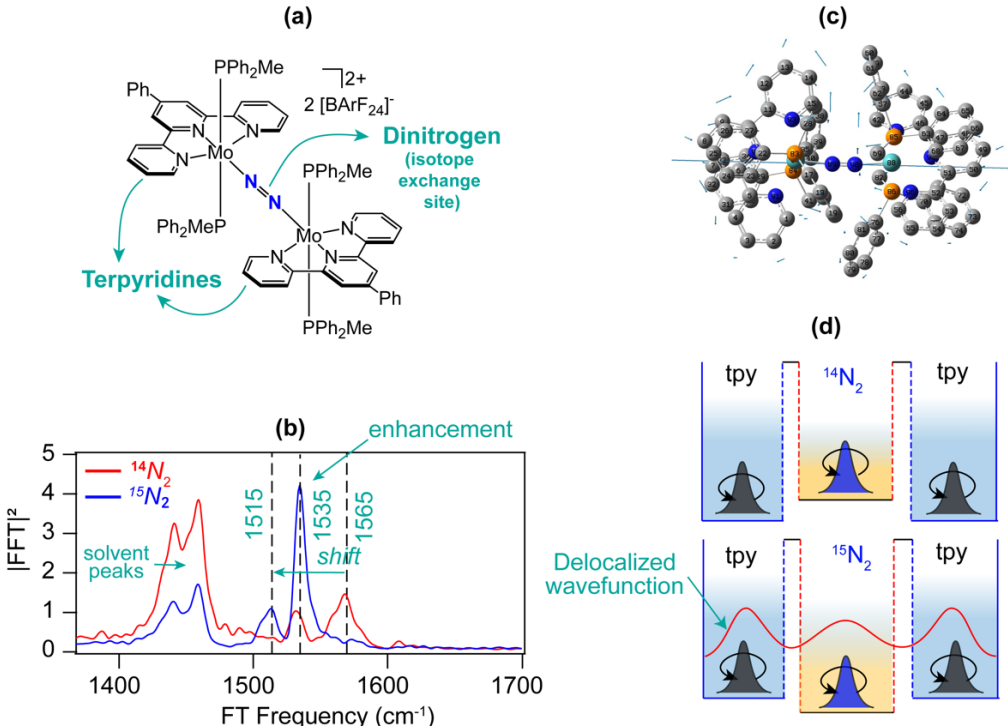


**Figure 5.** (a) Molecular structure of an end-on dinitrogen bridged bimetallic molybdenum complex supported by terpyridine and phosphine ligands. Two variants of this complex, differing by isotopic substitution at the dinitrogen site from  $^{14}N_2$  to  $^{15}N_2$  were investigated. (b) Fourier transform spectra of the two isotope analogs integrated over the measured probe frequency spectrum depicting the down of the dinitrogen stretching frequency and change in the intensity of the peak that lies between the frequencies of the lighter and heavier dinitrogen stretching frequencies. (c) The displacement vectors associated with the dinitrogen stretching mode are shown. The magnitude of these vectors over the terpyridine ligands was predicted, by theoretical calculations, to increase when dinitrogen was substituted from  $^{14}N_2$  to  $^{15}N_2$  in the complex. (d) A schematic illustration depicting the quantum mechanical mixing of vibrational wavefunctions extended from one terpyridine moiety to another via the dinitrogen due to Fermi-resonance coupling.

This mixing does not occur in the absence of the heavier dinitrogen isotope. Panel (a), (b), (c) are adapted with permission from ref. 3. Elsevier.

The energy coupling between the terpyridine in-plane vibration and the dinitrogen stretching vibration is provided by the onset of accidental quasi-resonance due to downshift in dinitrogen frequency. This, in the presence of anharmonic coupling, results in a Fermi-resonance like interaction.<sup>58</sup> Theoretical Raman calculations predicted a change in the transition polarizability tensor in the isotopically substituted complex. which has its origins in the quantum mechanical mixing of zero-order states via a higher order perturbation.<sup>59</sup> In principle, due to accidental Fermi-resonance, anharmonic coupling mixes vibrational wavefunctions of the two modes and therefore changes the transition polarizability, leading to wavepacket amplitude redistribution between the two vibrational wavepackets. This effect became strongly enhanced in the photo-excited state, supported by broadband pump probe and two-dimensional electronic spectroscopy.<sup>3</sup> An outcome of this interaction means that energy can be funneled from the in-plane terpyridine vibration to the dinitrogen stretching vibration without rapidly dissipating into the environment. Such couplings have been previously shown to result in energy buildup via intramolecular vibrational energy flow, leading to, for instance, the formation of H-Cl bond in the reaction between CHD<sub>3</sub> and Cl, or the dissociation of hydrogen peroxide via vibrational energy flow into O-O bond. 9, 60, 61 In general, such couplings reduce structural and thermodynamic barriers for vibrational energy flow, and selectively funnel energy into specific modes.<sup>62</sup>

The amplitude enhancement observed due to isotopic substitution can be contextualized by invoking wavepacket interference. The in-plane terpyridine vibration is in a localized basis on the individual terpyridines coordinated to the two molybdenum metal ions in the complex with  $^{14}N_2$  isotope, much like the overall vibrational mode being a linear combination of the two in-plane terpyridine modes. As discussed previously, due to the isotopic substitution at the dinitrogen site, the dinitrogen vibration couples to the terpyridine in-plane vibration, leading to spatial delocalization of wavepacket motion on the two spatially separated terpyridines. This extended delocalization introduces synchronized motion—mediated by the dinitrogen stretching vibration via wave function mixing—much like a constructive interference of the wavepacket on the terpyridines (Fig. 5d). This dynamic constructive interference leads to strong enhancement in the amplitude of the in-plane terpyridine vibration, without affecting the amplitude of the dinitrogen wavepacket drastically.

The support for this description can be borrowed from the observation that the Fermi-resonant interaction becomes more pronounced in the photoexcited state, and more importantly, it is a dynamic interaction that exists throughout the lifetime of the vibrational wavepackets during which the wavepacket can undergo constructive interference. This notion can be partly confirmed by comparing the ratio of the intensities of the in-plane terpyridine breathing and dinitrogen stretching vibration as obtained in resonance-Raman and time-resolved BBPP measurements. We observed that the ratio of the respective intensities was 1.38 in resonance-Raman, but increased to 3.96 when measured with BBPP.3 If this effect was solely a Franck-Condon phenomenon, then both resonance-Raman and BBPP should have yielded similar ratios because both techniques probe instantaneous change in the electronic polarizability induced by a molecular vibration. However, the BBPP approach yields a higher ratio of the intensities due to its time-resolved nature, which captures vibrational wavepackets as the system evolves beyond the Franck-Condon state, an aspect that the resonance-Raman technique overlooks. 63 An exact same laser pulse was employed to excite the two isotopes, ensuring that the experimental conditions are internally consistent, and the various vibrational wavepackets are driven to the same extent. Consequently, the BBPP technique can detect any time-dependent interaction of the wavepackets, including interference between them, leading to an increased intensity of the in-plane terpyridine vibrational wavepacket amplitude.

# 5. CONCLUSION AND OUTLOOK

In this account, we have described the advancements in our understanding of electronic-vibrational interplay that dictates the fate of photoinduced reactive dynamics. These advancements are based on tracking vibrational superposition states or wavepackets that are projected onto photoexcited states using ultrafast laser pulses. In particular, we track wavepackets along vibrations that are coupled to the electronic dynamics by monitoring certain key properties of wavepackets, for instance, their actively driven decoherence and dephasing, impulsive regeneration, and amplitude redistribution owing to redistribution in the constituent wavefunctions.

The research ideas covered in this account are a step towards a paradigm shift from confirming the existence of coherence in chemical systems to exploring the connection between coherence and function. In the example of binuclear platinum complexes, the decoherence or reemergence of coherence that ultimately fine tunes intersystem crossing dynamics in those complexes could be related to the steric bulkiness of the ligand system that holds the two monomeric units together. The future direction should focus on investigating extensive feedback between synthesis, experiment and theory, and the development of strategic and systematic methods to estimate the influence of coherence in specific functions. An example of that is the work reported by McCusker and coworkers, where they leveraged information obtained from vibronic coherence effects in the synthetic redesign of a transition metal complex with a longer lifetime in the excited state. 64 In another recent study by Rao and coworkers, the information afforded from vibrational coherences coupled to optical transitions was used to propose design rules that decouple excitons from high-frequency vibrations to minimize nonradiative losses. 65 This brings us to the realm of design-specific control over excited state properties based on principles inspired from quantum mechanics. Such control elements will give us access to fine tuning the interaction between various electronic states in the excited state manifold that could impact the outcome drastically. Thereby, allowing us wavefunction-level control over many technologically relevant processes ranging from singlet fission to thermally activated delayed fluorescence, and photocatalysis to quantum information.

To make further advancement in this area, novel theoretical methods that must go beyond simple population dynamics and explicitly include nuclear degrees and the associated structural changes is critical. We must also investigate similar processes in a manner where energy states—vibrational or electronic—are detuned from their molecular energies, thereby providing a means of elucidating the effect of changed vibrational or electronic gaps on the dynamics. This may be more crucial to determine the properties of wavepackets, especially dephasing dynamics, at detuned energies. One such paradigm where this can be achieved is strong light-matter coupling between molecular states and photon states in Fabry-Perot cavities.

# **Author Information Corresponding Authors**

Shahnawaz R. Rather - s.rather@uky.edu Gregory D. Scholes - gscholes@princeton.edu Lin X. Chen - lchen@northwestern.edu

### **Author contributions**

SRR led the preparation and writing of the original draft. All authors contributed to reviewing, rewriting and finalizing the manuscript.

### **Notes**

The authors declare no competing financial interests.

# **Biographies**

**Shahnawaz R. Rather** is an Assistant Professor of Chemistry at the University of Kentucky, USA. Originally from Kashmir, India, he received his Ph.D. in Chemistry from Indian Institute of technology Kanpur under the supervision of Prof. Pratik Sen. He then conducted postdoctoral research at Princeton

University under Prof. Greg Scholes, and at Northwestern University under Prof. Lin Chen focusing on ultrafast coherent spectroscopies to investigate the role of quantum coherence effects in photoinduced processes. His current research interests center on unravelling mechanisms and dynamics of energy conversion in molecules and materials using tools of ultrafast laser spectroscopy.

**Gregory D. Scholes** is the William S. Tod Professor of Chemistry at Princeton University. Originally from Melbourne, Australia, he later undertook postdoctoral training at Imperial College London and University of California Berkeley. He started his independent career at the University of Toronto (2000-2014) where he was the D.J. LeRoy Distinguished Professor. He was appointed Editor-in-Chief of the *Journal of Physical Chemistry Letters* in 2019. Dr. Scholes was elected a Fellow of the Royal Society (London) in 2019 and a Fellow of the Royal Society of Canada in 2009. He served as Chair of Department at Princeton 2020-2023 and Director of an Energy Frontier Research Center (BioLEC) since 2018.

Lin X. Chen is a Distinguished Fellow in Argonne National Laboratory and Professor of Chemistry in Northwestern University. After she received her Ph.D. from the University of Chicago and her postdoctoral training at UC Berkeley, she joined Argonne National Laboratory as a staff scientist, and later started a joined appointment with Northwestern University. She has been members of the Research Council for the Chemical, Biological and Geological Sciences Division, and Basic Energy Science Advisory Committee, Basic Energy Science, US Department of Energy, the Advisory Editorial Board of Journal of Physical Chemistry and Chemical Physics Letters, Journal of Materials Chemistry C, Aggregates, Senior Editor of ACS Energy Letters, Associate Editor of Chemical Science (RSC). She is an AAAS, RSC and ACA Fellow.

# Acknowledgment

The studies reviewed in this account were conducted by SRR and coauthors under the supervision of GDS at Princeton University and LXC at Northwestern University. The studies performed under the guidance of GDS at Princeton University were supported by the U.S. Department of Energy through grant no. DE-SC0015429. The research undertaken with LXC was supported at Northwestern University by the National Science Foundation under grant no. CHE-1955806, and at Argonne National Laboratory by the U.S. Department of Energy, Office of Science, Office of Basic Energy Sciences, Chemical, Biological, and Geological Sciences Division, through Argonne National Laboratory under contract DE-AC02-06CH11357.

### References

- (1) Rather, S. R.; Weingartz, N. P.; Kromer, S.; Castellano, F. N.; Chen, L. X. Spin-vibronic coherence drives singlet-triplet conversion. *Nature* **2023**, *620* (7975), 776-781.
- (2) Rather, S. R.; Fu, B.; Kudisch, B.; Scholes, G. D. Interplay of vibrational wavepackets during an ultrafast electron transfer reaction. *Nat. Chem.* **2021**, *13* (1), 70-76.
- (3) Rather, S. R.; Bezdek, M. J.; Chirik, P. J.; Scholes, G. D. Dinitrogen Coupling to a Terpyridine-Molybdenum Chromophore Is Switched on by Fermi Resonance. *Chem* **2019**, *5* (2), 402-416.
- (4) Crim, F. F. Chemical dynamics of vibrationally excited molecules: Controlling reactions in gases and on surfaces. *Proc. Natl. Acad. Sci. USA* **2008**, *105* (35), 12654-12661.
- (5) Crim, F. F. Vibrational state control of bimolecular reactions: Discovering and directing the chemistry. *Acc. Chem. Res.* **1999**, *32* (10), 877-884.
- (6) Hou, H.; Huang, Y.; Gulding, S. J.; Rettner, C. T.; Auerbach, D. J.; Wodtke, A. M. Enhanced reactivity of highly vibrationally excited molecules on metal surfaces. *Science* **1999**, *284* (5420), 1647-1650.
- (7) Beck, R. D.; Maroni, P.; Papageorgopoulos, D. C.; Dang, T. T.; Schmid, M. P.; Rizzo, T. R. Vibrational mode-specific reaction of methane on a nickel surface. *Science* **2003**, *302* (5642), 98-100.
- (8) Yan, S.; Wu, Y. T.; Zhang, B. L.; Yue, X. F.; Liu, K. P. Do vibrational excitations of CHD3 preferentially promote reactivity toward the chlorine atom? *Science* **2007**, *316* (5832), 1723-1726.

- (9) Hynes, J. T. Molecules in Motion: Chemical Reaction and Allied Dynamics in Solution and Elsewhere. *Annual Review of Physical Chemistry, Vol* 66 **2015**, 66, 1-20.
- (10) Rather, S. R.; Scholes, G. D. From Fundamental Theories to Quantum Coherences in Electron Transfer. *J. Am. Chem. Soc.* **2019**, *141* (2), 708-722.
- (11) Kumpulainen, T.; Lang, B.; Rosspeintner, A.; Vauthey, E. Ultrafast Elementary Photochemical Processes of Organic Molecules in Liquid Solution. *Chem Rev* **2017**, *117* (16), 10826-10939.
- (12) Mirkovic, T.; Ostroumov, E. E.; Anna, J. M.; van Grondelle, R.; Govindjee; Scholes, G. D. Light Absorption and Energy Transfer in the Antenna Complexes of Photosynthetic Organisms. *Chem Rev* **2017**, *117* (2), 249-293.
- (13) Welin, E. R.; Chip, L.; Daniela, M. A.-R.; James, K. M.; David, W. C. M. Photosensitized, energy transfer-mediated organometallic catalysis through electronically excited nickel(II). *Science* **2017**, *355*, 380-385.
- (14) Wasielewski, M. R.; Forbes, M. D. E.; Frank, N. L.; Kowalski, K.; Scholes, G. D.; Yuen-Zhou, J.; Baldo, M. A.; Freedman, D. E.; Goldsmith, R. H.; Goodson, T.; Kirk, M. L.; McCusker, J. K.; Ogilvie, J. P.; Shultz, D. A.; Stoll, S.; Whaley, K. B. Exploiting chemistry and molecular systems for quantum information science. *Nat. Rev. Chem.* **2020**, *4* (9), 490-504.
- (15) Goushi, K.; Yoshida, K.; Sato, K.; Adachi, C. Organic light-emitting diodes employing efficient reverse intersystem crossing for triplet-to-singlet state conversion. *Nat. Photonics* **2012**, *6* (4), 253-258.
- (16) Padgaonkar, S.; Olding, J. N.; Lauhon, L. J.; Hersam, M. C.; Weiss, E. A. Emergent Optoelectronic Properties of Mixed-Dimensional Heterojunctions. *Acc. Chem. Res.* **2020**, *53* (4), 763-772.
- (17) Nelson, T. R.; Ondarse-Alvarez, D.; Oldani, N.; Rodriguez-Hernandez, B.; Alfonso-Hernandez, L.; Galindo, J. F.; Kleiman, V. D.; Fernandez-Alberti, S.; Roitberg, A. E.; Tretiak, S. Coherent exciton-vibrational dynamics and energy transfer in conjugated organics. *Nat. Commun.* **2018**, *9*.
- (18) Falke, S. M.; Rozzi, C. A.; Brida, D.; Maiuri, M.; Amato, M.; Sommer, E.; Sio, A. D.; Rubio, A.; Cerullo, G.; Molinari, E.; Lienau, C. Coherent ultrafast charge transfer in an organic photovoltaic blend. *Science* **2014**, *344* (6187), 1001-1005.
- (19) Scholes, G. D.; Fleming, G. R.; Chen, L. X.; Aspuru-Guzik, A.; Buchleitner, A.; Coker, D. F.; Engel, G. E.; van Grondelle, R.; Ishizaki, A.; Jonas, D. M.; Lundeen, J. S.; McCusker, J. K.; Mukamel, S.; Ogilvie, J. P.; Olaya-Castro, A.; Ratner, M. A.; Spano, F. C.; Whaley, K. B.; Zhu, X. Utilizing Coherence to Enhance Function in Chemical and Biophysical Systems. *Nature (London)* **2017**, *543*, 647-656.
- (20) Wang, L. L.; Allodi, M. A.; Engel, G. S. Quantum coherences reveal excited-state dynamics in biophysical systems. *Nat. Rev. Chem.* **2019**, *3* (8), 477-490.
- (21) Engel, G. S.; Calhoun, T. R.; Read, E. L.; Ahn, T.-K.; Mancal, T.; Cheng, Y.-C.; Blankenship, R. E.; Fleming, G. R. Evidence for wavelike energy transfer through quantum coherence in photosynthetic systems. *Nature* **2007**, 446 (7137), 782-786.
- (22) Collini, E.; Wong, C. Y.; Wilk, K. E.; Curmi, P. M. G.; Brumer, P.; Scholes, G. D. Coherently wired light-harvesting in photosynthetic marine algae at ambient temperature. *Nature* **2010**, *463* (7281), 644-647.
- (23) Jumper, C. C.; Rather, S. R.; Wang, S.; Scholes, G. D. From coherent to vibronic light harvesting in photosynthesis. *Curr. Opin. Chem. Biol.* **2018**, *47*, 39-46.
- (24) Dean, J. C.; Mirkovic, T.; Toa, Z. S. D.; Oblinsky, D. G.; Scholes, G. D. Vibronic Enhancement of Algae Light Harvesting. *Chem* **2016**, *I* (6), 858-872.
- (25) Polli, D.; Altoe, P.; Weingart, O.; Spillane, K. M.; Manzoni, C.; Brida, D.; Tomasello, G.; Orlandi, G.; Kukura, P.; Mathies, R. A.; Garavelli, M.; Cerullo, G. Conical intersection dynamics of the primary photoisomerization event in vision. *Nature* **2010**, *467* (7314), 440-443.
- (26) Johnson, P. J. M.; Halpin, A.; Morizumi, T.; Prokhorenko, V. I.; Ernst, O. P.; Miller, R. J. D. Local vibrational coherences drive the primary photochemistry of vision. *Nat. Chem.* **2015**, *7* (12), 980-986.
- (27) Musser, A. J.; Liebel, M.; Schnedermann, C.; Wende, T.; Kehoe, T. B.; Rao, A.; Kukura, P. Evidence for conical intersection dynamics mediating ultrafast singlet exciton fission. *Nature Physics* **2015**, *11* (4), 352-357.
- (28) Fuller, F. D.; Pan, J.; Gelzinis, A.; Butkus, V.; Senlik, S. S.; Wilcox, D. E.; Yocum, C. F.; Valkunas, L.; Abramavicius, D.; Ogilvie, J. P. Vibronic coherence in oxygenic photosynthesis. *Nat. Chem.* **2014**, *6* (8), 706-711.
- (29) Romero, E.; Augulis, R.; Novoderezhkin, V. I.; Ferretti, M.; Thieme, J.; Zigmantas, D.; van Grondelle, R.
- Quantum coherence in photosynthesis for efficient solar-energy conversion. *Nature Physics* **2014**, *10* (9), 677-683. (30) Rozzi, C. A.; Falke, S. M.; Spallanzani, N.; Rubio, A.; Molinari, E.; Brida, D.; Maiuri, M.; Cerullo, G.;
- Schramm, H.; Christoffers, J.; Lienau, C. Quantum coherence controls the charge separation in a prototypical artificial light-harvesting system. *Nat Commun* **2013**, *4*, 1602.
- (31) Gelinas, S.; Rao, A.; Kumar, A.; Smith, S. L.; Chin, A. W.; Clark, J.; van der Poll, T. S.; Bazan, G. C.; Friend, R. H. Ultrafast Long-Range Charge Separation in Organic Semiconductor Photovoltaic Diodes. *Science* **2014**, *343* (6170), 512-516.

- (32) Chenu, A.; Scholes, G. D. Coherence in Energy Transfer and Photosynthesis. *Annu. Rev. Phys. Chem.* **2015**, *66*, 69-96.
- (33) Rather, S. R.; Scholes, G. D. Slow Intramolecular Vibrational Relaxation Leads to Long-Lived Excited-State Wavepackets. *J. Phys. Chem. A* **2016**, *120* (34), 6792-6799.
- (34) McClure, S. D.; Turner, D. B.; Arpin, P. C.; Mirkovic, T.; Scholes, G. D. Coherent Oscillations in the PC577 Cryptophyte Antenna Occur in the Excited Electronic State. *J. Phys. Chem. B* **2014**, *118* (5), 1296-1308.
- (35) Jonas, D. M. Two-dimensional femtosecond spectroscopy. Annu. Rev. Phys. Chem. 2003, 54, 425-463.
- (36) Jonas, D. M. Vibrational and Nonadiabatic Coherence in 2D Electronic Spectroscopy, the Jahn-Teller Effect, and Energy Transfer. *Annual Review of Physical Chemistry, Vol 69* **2018**, *69*, 327-352.
- (37) Rather, S. R.; Dean, J. C.; Scholes, G. D. Observing Vibrational Wavepackets during an Ultrafast Electron Transfer Reaction. *J. Phys. Chem. A* **2015**, *119* (49), 11837-11846.
- (38) Dean, J. C.; Rather, S. R.; Oblinsky, D. G.; Cassette, E.; Jumper, C. C.; Scholes, G. D. Broadband Transient Absorption and Two-Dimensional Electronic Spectroscopy of Methylene Blue. *The Journal of Physical Chemistry A* **2015**, *119* (34), 9098-9108.
- (39) Johnson, P. J.; Halpin, A.; Morizumi, T.; Prokhorenko, V. I.; Ernst, O. P.; Miller, R. J. Local vibrational coherences drive the primary photochemistry of vision. *Nat Chem* **2015**, *7* (12), 980-986.
- (40) Domcke, W.; Stock, G. Theory of Ultrafast Nonadiabatic Excited-State Processes and Their Spectroscopic Detection in Real Time. *Adv. Chem. Phys.* **1997**, *100*, 1-169.
- (41) Albrecht, A. C. Vibronic—Spin Orbit Perturbations and the Assignment of the Lowest Triplet State of Benzene. *J. Chem. Phys.* **1963**, *38* (2), 354-365.
- (42) Penfold, T. J.; Gindensperger, E.; Daniel, C.; Marian, C. M. Spin-Vibronic Mechanism for Intersystem Crossing. *Chem. Rev.* **2018**, *118* (15), 6975-7025.
- (43) Cannizzo, A.; Blanco-Rodríguez, A. M.; El Nahhas, A.; Šebera, J.; Záliš, S.; Vlček, A., Jr.; Chergui, M. Femtosecond Fluorescence and Intersystem Crossing in Rhenium(I) Carbonyl–Bipyridine Complexes. *J. Am. Chem. Soc.* **2008**, *130* (28), 8967-8974.
- (44) Kim, J.; Kang, D.-g.; Kim, S. K.; Joo, T. Role of coherent nuclear motion in the ultrafast intersystem crossing of ruthenium complexes. *Physical Chemistry Chemical Physics* **2020**, *22* (44), 25811-25818.
- (45) Auböck, G.; Chergui, M. Sub-50-fs photoinduced spin crossover in [Fe(bpy)3]2+. Nat. Chem. 2015, 7 (8), 629-633.
- (46) Etherington, M. K.; Gibson, J.; Higginbotham, H. F.; Penfold, T. J.; Monkman, A. P. Revealing the spin–vibronic coupling mechanism of thermally activated delayed fluorescence. *Nat. Commun.* **2016**, *7* (1), 13680.
- (47) Tatchen, J.; Gilka, N.; Marian, C. M. Intersystem crossing driven by vibronic spin–orbit coupling: a case study on psoralen. *Physical Chemistry Chemical Physics* **2007**, *9* (38), 5209-5221.
- (48) Saito, K.; Nakao, Y.; Sakaki, S. Theoretical Study of Pyrazolate-Bridged Dinuclear Platinum(II) Complexes: Interesting Potential Energy Curve of the Lowest Energy Triplet Excited State and Phosphorescence Spectra. *Inorg. Chem.* **2008**, *47* (10), 4329-4337.
- (49) Kim, P.; Valentine, A. J. S.; Roy, S.; Mills, A. W.; Chakraborty, A.; Castellano, F. N.; Li, X.; Chen, L. X. Ultrafast Excited-State Dynamics of Photoluminescent Pt(II) Dimers Probed by a Coherent Vibrational Wavepacket. *J. Phys. Chem. Lett.* **2021**, *12* (29), 6794-6803.
- (50) Monni, R.; Capano, G.; Auböck, G.; Gray, H. B.; Vlček, A.; Tavernelli, I.; Chergui, M. Vibrational coherence transfer in the ultrafast intersystem crossing of a diplatinum complex in solution. *Proc. Natl. Acad. Sci.* **2018**.
- (51) Duan, H.-G.; Thorwart, M. Quantum Mechanical Wave Packet Dynamics at a Conical Intersection with Strong Vibrational Dissipation. *J. Phys. Chem. Lett.* **2016**, *7* (3), 382-386.
- (52) Rather, S. R.; Scholes, G. D. Is back-electron transfer process in Betaine-30 coherent? *Chem. Phys. Lett.* **2017**, 683, 500-506.
- (53) Jortner, J.; Bixon, M. Intramolecular vibrational excitations accompanying solvent-controlled electron transfer reactions. *J. Chem. Phys.* **1988**, *88*, 167-170.
- (54) Yoneda, Y.; Kudisch, B.; Rather, S. R.; Maiuri, M.; Nagasawa, Y.; Scholes, G. D.; Miyasaka, H. Vibrational Dephasing along the Reaction Coordinate of an Electron Transfer Reaction. *J. Am. Chem. Soc.* **2021**, *143* (36), 14511-14522.
- (55) Egorova, D.; Kuhl, A.; Domcke, W. Modeling of ultrafast electron-transfer dynamics: multi-level Redfield theory and validity of approximations. *Chem. Phys.* **2001**, *268* (1-3), 105-120.
- (56) Rather, S. R.; Bezdek, M. J.; Koch, M.; Chirik, P. J.; Scholes, G. D. Ultrafast Photophysics of a Dinitrogen-Bridged Molybdenum Complex. *J. Am. Chem. Soc.* **2018**, *140* (20), 6298-6307.

- (57) Bezdek, M. J.; Guo, S.; Chirik, P. J. Terpyridine Molybdenum Dinitrogen Chemistry: Synthesis of Dinitrogen Complexes That Vary by Five Oxidation States. *Inorg. Chem.* **2016**, *55* (6), 3117-3127.
- (58) Sibert, E. L.; Hynes, J. T.; Reinhardt, W. P. Fermi Resonance from a Curvilinear Perspective. *J. Phys. Chem.* **1983**, *87* (12), 2032-2037.
- (59) Monecke, J. Theory of Fermi Resonances in Raman and Infrared-Spectra. J. Raman Spectrosc. 1987, 18 (7), 477-479.
- (60) Rizzo, T. R.; Hayden, C. C.; Crim, F. F. State-Resolved Product Detection in the Overtone Vibration Initiated Unimolecular Decomposition of Hooh(6-Nu-Oh). *J. Chem. Phys.* **1984**, *81* (10), 4501-4509.
- (61) Yan, S.; Wu, Y. T.; Liu, K. Tracking the energy flow along the reaction path. *Proc. Natl. Acad. Sci. USA* **2008**, *105* (35), 12667-12672.
- (62) Jakob, P. Fermi resonance distortion of the Ru-CO stretching mode of CO adsorbed on Ru(001). *J. Chem. Phys.* **1998**, *108* (12), 5035-5043.
- (63) Hupp, J. T.; Williams, R. D. Using resonance Raman spectroscopy to examine vibrational barriers to electron transfer and electronic delocalization. *Acc. Chem. Res.* **2001**, *34* (10), 808-817.
- (64) Paulus, B. C.; Adelman, S. L.; Jamula, Lindsey L.; McCusker, James K. Leveraging excited-state coherence for synthetic control of ultrafast dynamics. *Nature* **2020**, *582* (7811), 214-218.
- (65) Ghosh, P.; Alvertis, A. M.; Chowdhury, R.; Murto, P.; Gillett, A. J.; Dong, S.; Sneyd, A. J.; Cho, H.-H.; Evans, E. W.; Monserrat, B.; Li, F.; Schnedermann, C.; Bronstein, H.; Friend, R. H.; Rao, A. Decoupling excitons from high-frequency vibrations in organic molecules. *Nature* **2024**, *629* (8011), 355-362.

# **TOC Graphic**

